HHS Public Access

Author manuscript

Cell Host Microbe. Author manuscript; available in PMC 2019 October 10.

Published in final edited form as:

Cell Host Microbe. 2018 October 10; 24(4): 487–499.e5. doi:10.1016/j.chom.2018.09.008.

A single-dose live-attenuated Zika virus vaccine with controlled infection rounds that protects against vertical transmission

Xuping Xie[1,*], **Dieudonné B. Kum**[2], **Hongjie Xia**[1], **Huanle Luo**[7], **Chao Shan**[1], **Jing Zou**[1], **Antonio E. Muruato**[1], **Daniele B. A. Medeiros**[1,3], **Bruno T. D. Nunes**[1,3], **Kai Dallmeier**[2], **Shannan L. Rossi**[5,8], **Scott C. Weaver**[5,6,7,8,9], **Johan Neyts**[2], **Tian Wang**[7,8,9], **Pedro F. C. Vasconcelos**[3,4], and **Pei-Yong Shi**[1,9,10,11,*]

[1]Department of Biochemistry & Molecular Biology, University of Texas Medical Branch, Galveston, Texas, USA

[2]KU Leuven, Rega Institute for Medical Research, Department of Microbiology and Immunology, Laboratory of Virology and Chemoth, University of Leuven, Leuven, Belgium

[3]Department of Arbovirology and Hemorrhagic Fevers, Evandro Chagas Institute, Ministry of Health, Ananindeua, Pará State, Brazil

[4]Department of Pathology, Pará State University, Belém, Brazil

[5]Institute for Human Infections & Immunity, University of Texas Medical Branch, Galveston, Texas, USA

[6]Institute for Translational Sciences, University of Texas Medical Branch, Galveston, Texas, USA

[7]Department of Microbiology & Immunology, University of Texas Medical Branch, Galveston, Texas, USA

[8]Department of Pathology and Center for Biodefense & Emerging Infectious Diseases, University of Texas Medical Branch, Galveston, Texas, USA

[9]Sealy Institute for Vaccine Sciences, University of Texas Medical Branch, Galveston, Texas, USA

[10]Sealy Center for Structural Biology & Molecular Biophysics, University of Texas Medical Branch, Galveston, Texas, USA

[*]Correspondence: xuxie@utmb.edu or peshi@utmb.edu.
Lead contact: peshi@utmb.edu

Author Contributions

X.X., D.B.K., H.X., H.L., C.S., J.Z., A.E.M., D.M., B.D., T.W. performed experiments and data analysis. X.X., D.B.K., H.X. and P.Y.S. designed the experiments and interpreted the results. X.X., D.B.K., H.X., K.D., S.L.R., S.C.W., T.W., J.N., P.F.C.V. and P.Y.S. wrote the manuscript.

Declaration of Interests

The authors declare no competing interests.

Data and Software Availability

The raw Western Blot data (related to Figure 3h) can be accessed through DOI: 10.17632/9ngf9wmj4f.1 in the Mendeley Data.

[11]Department of Pharmacology & Toxicology, University of Texas Medical Branch, Galveston, Texas, USA

Summary

Zika virus (ZIKV) infection of the mother during pregnancy causes devastating Zika congenital syndrome in the offspring. A ZIKV vaccine with optimal safety and immunogenicity for use in pregnant women is critically needed. Towards this goal, we have developed a singledose live-attenuated vaccine candidate that infects cells with controlled, limited infection rounds. The vaccine contains a 9-amino acid deletion in the viral capsid protein, and replicates to titers of $>10^6$ focus-forming units (FFU)/ml in cells expressing the full-length capsid protein. Immunization of A129 mice with one dose (10^5 FFU) did not produce viremia, but elicited protective immunity that completely prevented viremia, morbidity, and mortality after challenge with an epidemic ZIKV strain (10^6 PFU). A single-dose vaccination also fully prevented infection of pregnant mice and maternal-to-fetal transmission. Intracranial injection of the vaccine (10^4 FFU) to one-day-old mice did not cause any disease or death, underscoring the safety of this vaccine candidate.

In Brief

A ZIKV vaccine for use in pregnant women requires an optimal balance between safety and immunogenicity. Xie et al. developed a live-attenuated vaccine candidate that can infect cells with controlled, limited infection rounds. A single-dose immunization of the vaccine prevents vertical transmission of ZIKV in pregnant mice.

Graphical abstract

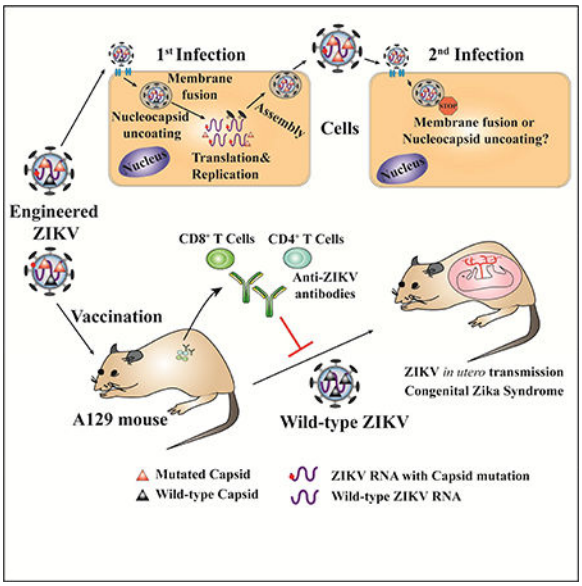

Keywords

Zika virus; vaccine; flavivirus capsid

Introduction

Zika virus (ZIKV) is a newly emerged flavivirus that is primarily transmitted by mosquitoes, but can also be acquired through sexual, vertical, and blood transfusion routes (Aliota et al., 2017). Besides ZIKV, many flaviviruses are significant human pathogens, including dengue (DENV), yellow fever (YFV), Japanese encephalitis (JEV), West Nile (WNV), and tickborne encephalitis (TBEV) viruses (Shan et al., 2016a). Flaviviruses have a single-stranded, positive-sense RNA genome containing a 5' untranslated region (UTR), a single open-readingframe, and a 3'UTR. The open-reading-frame encodes three structural [capsid (C), premembrane (prM), and envelope (E)] and seven nonstructural (NS1-NS2A-NS2B-NS3-NS4ANS4B-NS5) proteins. The structural proteins together with viral RNA form virions, while the nonstructural proteins participate in viral replication, assembly, and evasion of the host immunity (Pierson and Diamond, 2013).

The most devastating manifestations of ZIKV infection are Guillain-Barré syndrome in adults (Cao-Lormeau et al., 2016) and congenital Zika syndrome (CZS) in infants born to women infected during pregnancy (Brasil et al., 2016; Rasmussen et al., 2016). Currently, no licensed vaccines or drugs are available to prevent ZIKV infection (Shan et al., 2018a; Xie et al., 2017b). Several ZIKV vaccine candidates have been developed, including inactivated, subunit (prM-E proteins expressed from DNA, RNA, or viral vectors), and live-attenuated vaccines (LAVs) (Abbink et al., 2016; Betancourt et al., 2017; Dowd et al., 2016; Larocca et al., 2016; Li et al., 2018b; Pardi et al., 2017; Richner et al., 2017b; Shan et al., 2017a; Shan et al., 2017b; Shan et al., 2018a; Xie et al., 2017a), several of which have already entered phase I/II clinical trials (Gaudinski et al., 2017; Modjarrad et al., 2017; Tebas et al., 2017). Different vaccine platforms have their intrinsic strengths and weaknesses. Inactivated and subunit vaccines are safe, but often require multiple initial doses and periodic boosting. LAVs typically require only a single dose, induce rapid and durable immunity, can be manufactured at a low cost, but have potential safety liabilities, particularly when used in immune-deficient and pregnant individuals. However, since ZIKV is endemic primarily in developing countries, a vaccine with single-dose efficacy is of practical importance, particularly when immunizing mass populations in remote areas.

The flavivirus C is a positively charged protein containing an N-terminal unstructured region, a pre-α1 loop, and four helices (Fig. 1a). The four helices facilitate the dimerization of the C protein (Dokland et al., 2004; Li et al., 2018a; Ma et al., 2004; Shang et al., 2018). Helices α2 and α3 are hydrophobic and can bind lipid-membrane, while helix α4 forms the main RNA-binding interface. Previous studies showed that deletions of helices α2 and α3 impair virion production in TBEV, YFV, WNV, and DENV-2 (Kofler et al., 2002; Patkar et al., 2007; Schlick et al., 2009; Zhu et al., 2007). The length and position of the C deletion determine the level of virion assembly, ranging from a slight decrease to complete abolishment of infectious virus assembly. These findings have informed two vaccine approaches. Approach I uses C-deletion mutants that are reduced in forming infectious viruses; these mutant viruses infect cells for multiple rounds, but at reduced levels than the wild-type (WT) virus (Kofler et al., 2004; Schlick et al., 2010). Approach II uses C-deletion mutants that could not form infectious viruses; such mutant RNAs can be packaged into pseudo-infectious particles (PIP) by *trans* supplying full-length C proteins; the PIPs can

infect cells for single round (due to the C-deletion in viral genome) to elicit protective immunity (Chang et al., 2008; Widman et al., 2008; Widman et al., 2009). In this study, we analyzed the function of the C protein in ZIKV assembly and rationally developed a C-deletion ZIKV with controlled infection rounds as a potent and safe vaccine.

Results

Characterization of C-deletion ZIKVs in cell culture

Since previous studies showed that helices α2 and α3 of the C protein are important for flavivirus assembly, we probed the function of the ZIKV C protein by introducing various deletions, located mainly at these two helices, into a cDNA clone of Cambodian strain FSS13025 (Shan et al., 2016b). We chose this pre-epidemic ZIKV strain because, compared with epidemic American isolates, the FSS13025 strain is attenuated in neurovirulence, immune antagonism, and mosquito infectivity (Liu et al., 2017; Xia et al., 2018; Yuan et al., 2017), making it a safe starting point for vaccine development. Three panels of deletion mutants were prepared (Fig. 1b): Panel I contains six mutants (C1 to C6) with deletions of residues 7–20 in the α2 helix; panel II contains seven mutants (C7 to C13) with deletions of residues 4–9 in the α3 helix; and panel III contains three mutants (C14 to C-16) with larger deletions of residues 25–74 spanning the entire capsid. To examine the effect of these deletions on virion assembly, we transfected equal amounts of viral RNAs into Vero cells and monitored viral NS3 protein expression (Fig. 1c and Fig. S1). All deletion RNAs generated NS3-positive cells. However, none of the transfected cells showed increasing numbers of NS3-positive cells from day 1 to day 3 post-transfection (p.t.), suggesting no spread of infectious viruses. When supernatants from the transfected cells were used to infect naïve Vero cells, only mutant C12 generated infectious virus with a low titer (1.5×10^2 IFU/ml). No other mutants produced detectable infectious viruses (Fig. 1d, e). To examine if mutant RNAs were packaged into virions that were not infectious, we quantified the viral RNA in culture medium using real-time RT-PCR. All mutants from panel II, but none from panels I or III, secreted viral RNAs into culture medium (Fig. 1f); RNase A treatment of the supernatant from the panel II RNA-transfected cells did not reduce the real-time RT-PCR signals (data not shown), suggesting that viral RNAs were enclosed in the form of virions. As controls, ZIKV replicon RNA-transfected cells did not generate any infectious or non-infectious viruses in the supernatant, whereas WT viral RNA-transfected cells produced 5×10^6 IFU/ml infectious virus (Fig. 1d, e). Collectively, these results indicate that, except for C12, other C deletions abolished infectious virus production, among which panel II mutants may form non-infectious virions. It should be noted that the ZIKV data presented here are in contrast to the previously reported C-deletion results for TBEV, YFV, and WNV, all of which could tolerate C deletions and produce infectious viruses (Kofler et al., 2002; Patkar et al., 2007; Schlick et al., 2009).

Effects of C deletion on virion assembly and infection

To further define the effects of C deletions on ZIKV assembly and release, we performed experiments outlined in Fig. S2a. We chose the C7 deletion for this analysis because this mutant generated the highest level of non-infectious virions, as evidenced by the highest level of extracellular viral RNA (Fig. 1f). Equal amounts of C7 viral RNA, WT viral RNA,

and replicon RNA were electroporated into Vero cells. At 48 h p.t., intracellular and extracellular viral RNA levels were measured by real-time RT-PCR. Although the intracellular level of C7 RNA was lower than that of replicon RNA (Fig. S2b, left panel), the extracellular level of C7 RNA was >100-fold higher than that of replicon RNA (Fig. S2b, right panel), indicating that C7 RNA was assembled into virions and released into the supernatant. Notably, although both the intracellular and extracellular levels of C7 RNA were significantly lower than those of WT RNA, the ratios of extracellular to intracellular RNA levels were comparable for C7 and WT (Fig. S2c), suggesting that the C7 deletion does not significantly reduce the efficiency of virion assembly and release.

To identify which steps were blocked during C7 virion infection, Vero cells were infected with equal amounts of C7 and WT virions (quantified by viral RNA levels) recovered from the viral RNA-transfected Vero cells (P0 virus; Fig. S2a). The infected cells were quantified for levels of intracellular and extracellular viral RNAs (Fig. S2d). At 1 h post-infection (p.i.), comparable levels of intracellular viral RNAs were detected for C7 and WT virion infections (Fig. S2d, left panel), suggesting that both virions could enter cells at a similar efficiency. Corroboratively, C7 and WT virions bound to Vero cells at equivalent efficiencies at 4°C (Fig. S2e). At 24 and 48 h p.i., the intracellular C7 RNA did not increase and the extracellular C7 RNA was below the limit of detection; in contrast, intracellular WT RNA levels increased by >1,000 fold (compared with the viral RNA level at 1 h p.i.), generating $>10^7$ copies/ml of extracellular WT RNA (Fig. S2d). These results suggest that the C7 virion can attach and enter cells, but cannot initiate RNA synthesis afterwards, possibly due to defects in membrane fusion and/or nucleocapsid un-coating. As expected, incubation of naïve Vero cells with P1 supernatant did not yield any intracellular C7 RNA replication (Fig. S2f).

Production of infectious C-deletion virus through *trans* complementation

To rescue infectious viruses for the C deletion mutants, we prepared a stable BHK-21 cell line that constitutively expressed a full-length C protein fused with an N-terminal HA tag (BHK-HA-C; Fig. S3a). Each BHK-HA-C cell expressed the HA-C fusion protein located in both the cytoplasm and nucleus (Fig. S3b). We compared the *trans* complementation efficiencies of all deletion mutants by transfecting equal amounts of viral RNAs into the BHK-HA-C cells. The transfected cells were monitored for viral E-positive cells from day 1 to day 3 p.t. (Fig. S3c-e). A slight increase of E-positive cells was observed on C1–5 (Fig. S3c) and C14–16 (Fig. S3e) RNA-transfected cells, suggesting marginal restoration of virion infectivity and spread. In contrast, C6–13 deletion RNA-transfected cells showed significant increases in E-positive cells from day 1 to 3 p.t. (Fig. S3c, d), suggesting efficient rescue of virion infectivity and spread. Given that C7 contained the largest deletion (thus a lower chance of reverting to WT) and retained efficient replication in the BHK-HA-C cells (beneficial for virus production), we decided to focus on this mutant in the following experiments.

We characterized the *trans* complementation of the C7 mutant in more details. In agreement with Fig. S3, transfection of C7 RNA into BHK-HA-C cells generated increasing numbers of viral E protein-positive cells from day 1 to 4 (Fig. 2a, third panel), and produced C7t virus

("t" representing "*trans* complemented") that can infect naïve BHK-21 cells (Fig. 2b, third panel). The C7t virus could form small infectious foci on BHK-HA-C cells (Fig. 2c, third panel), but not on naïve BHK-21 cells (Fig. 2c, first panel). The *trans* complementation produced 1.4×10^4 FFU/ml of C7t virus (Fig. 2d). As a positive control, WT RNA generated infectious virus that could infect and spread on both naïve BHK-21 and BHK-HA-C cells (Fig. 2a-d).

To improve the yields of *trans* complementation, we passaged the C7t virus on BHK-HAC cells for 8 consecutive rounds (P0 to P8; Fig. 2e). Compared with P0 C7t virus, P8 C7t virus produced larger infectious foci (compare Fig. 2f with 2c, third panel) and a ~100-fold higher infectious titer to 1.2×10^6 FFU/ml (Fig. 2g). Sequencing the whole genome of P8 C7t virus revealed three adaptive mutations in addition to the original C7 deletion: E21K in prM, E27G in NS2B, and one synonymous mutation in NS5 (Fig. 2h). These results demonstrate that (i) an adaptive C7t virus (*i.e.*, C7a/t virus, "a/t" representing "adaptive/*trans* complemented") can be selected and (ii) such C7a/t virus could be produced to a high yield on BHK-HA-C cells through *trans* complementation.

Analysis of adaptive mutations in cell culture

To validate the role of adaptive mutations in C7a/t production, we engineered both prM E21K and NS2B E27G into the infectious clone of ZIKV strain FSS13025 (Shan et al., 2016b). We first compared the specific infectivity of C7 and C7a (containing the two adaptive mutations) RNAs on BHK-HA-C cells (Fig. 3a, upper-left panel). The specific infectivity is defined as the number of infectious viruses produced after transfecting 1 μg of viral RNA into cells. The specific infectivity of C7a RNA was similar to that of WT viral RNA, which was 2-fold higher than that of C7 RNA (Fig. 3a, upper-right panel). Notably, the specific infectivity assay showed plaque sizes in the order of WT ZIKV > C7a virus > C7 virus (Fig. 3a, lower panel). These results suggest that the two adaptive mutations improve the specific infectivity of C7 mutant, leading to a higher yield of C7a/t virus on BHK-HA-C cells.

Next, we characterized the replication of C7a RNA on Vero, BHK-21, and BHK-HA-C cells (Fig. 3b, c). As expected, after transfecting C7a RNA into Vero cells, no increase in viral E-positive cells was observed from day 1 to 4 p.t., yielding no detectable infectious virus (Fig. 3c, left panel). On BHK-HA-C cells, increasing numbers of E-positive cells were observed, yielding 1.6×10^6 FFU/ml of infectious C7a/t virus on day 4 p.t. (Fig. 3b, right panel). Surprisingly, on naïve BHK-21 cells, an increasing number of E-positive cells was also observed, producing 1.2×10^5 FFU/ml of C7a virus (Fig. 3b, c, middle panels). Congruently, the C7a/t virus formed infectious foci on BHK-21 and BHK-HA-C cells, but not on Vero cells (Fig. 3d). Furthermore, the C7a/t virus replicated to a titer of 3×10^5 FFU/ml on BHK-21 cells, but only to a titer of 300 FFU/ml on Vero cells (using BHK-HA-C cells for quantifying infectious viruses); as a positive control, WT ZIKV replicated to higher titers of 8×10^5 FFU/ml and 7×10^6 FFU/ml on BHK-21 and Vero cells, respectively (Fig. 3e). These results demonstrate that C7a/t virus is fully infectious on BHK-21 cells, but not on Vero cells.

To examine if C7a/t virus is also fully infectious on other cell types, we tested five more human cell lines (A549, alveolar epithelial cell; Hela, cervix epithelial cell; JEG-3, placenta epithelial cell; HTB-8/SVneo, placenta trophoblast cell; and HTB-15, brain glioblastoma cell) and one mouse cell line (myoblast C2C12). As a positive control, WT ZIKV infected all cell lines and spread to more cells from day 1 to 3, although the percentages of E-positive cells varied among different cell lines (Fig. 3f). The C7a/t virus also infected all cell lines with varied efficiencies, but the percentages of E-positive cells decreased from day 1 to day 3 p.i. (Fig. 3g), suggesting no spread of the C7a/t virus on these cells. Collectively, these results demonstrate that these adaptive mutations (prM E21K and NS2B E27G) confer full infection only on BHK-21 cells (where the adaptive mutations were selected from), but not on the other tested cell lines.

To understand the restricted spread of C7a/t infection, we examined the viral entry, RNA synthesis, and virion production of C7a/t on Vero or A549 cells. At 1 h p.i., comparable levels of viral RNAs were detected in cells infected with C7a/t and WT virus (Fig. S4a, c), suggesting that C7a/t virus is not defective in viral entry. In the C7a/t virus-infected cells, intracellular viral RNA increased from 4 to 16 h, and plateaued from 16 to 48 h p.i.; low levels of progeny C7a virus ($<4\times10^2$ FFU/ml when measured on BHK-HA-C cells) were released to supernatant (Fig. S4b, d). Compared with the C7a/t infection, WT ZIKV produced significantly more intracellular viral RNA and extracellular virus, both of which increased continuously from 4 to 48 h post-infection. These results indicate that C7a/t virus could efficiently enter cells, replicate its viral RNA, and produce a low level of C7a virus; however, the progeny C7a virus cannot launch a productive infection cycle after entering cells, as demonstrated in Fig. S2.

Requirement of complete ZIKV C protein in C7a/t virus for productive infections

We analyzed the composition of C protein variants in C7a/t virus using Western blot. As shown in Fig. 3h, the C7a/t virus contained two C variants: HA-C (~12.5 kDa) and C7 (~10.5 kDa) proteins with an estimated molecular ratio of 1:30, whereas the WT ZIKV had only full-length C protein (~11.4 kDa). As expected, both C7a/t and WT viruses contained mature M and E proteins. As controls, supernatant from replicon-transfected cells contained only NS1 protein, with no detectable structural proteins (C, M, or E). The data suggest that (i) C7a/t ZIKV contains both HA-C and C7 proteins and (ii) the presence of HA-C protein may facilitate viral replication after entry.

Next, we asked if C7a/t virus could be rescued through *trans* complementation from cells that are co-infected with other flaviviruses. Vero cells were co-infected with C7a/t virus and DENV-2 (MOI of 5.0). At 48 h p.i., supernatant (P1) was collected to infect naïve Vero cells. After 48 h of P1 infection, supernatant (P2) was harvested and tested for ZIKV RNA by real-time RT-PCR. No ZIKV RNA was detected in the P2 supernatant (data not shown). This result suggests no *trans* complementation between ZIKV C7a and DENV-2 C protein in the co-infected cells.

Stability of C7a/t virus

We evaluated the genetic stability of C7a/t virus when produced on BHK-HA-C cells. After 10 rounds of consecutive culturing on BHK-HA-C cells, the C7a/t virus did not change its focus morphology on BHK-HA-C cells (Fig. S5a). Sequencing the complete genome of P10 virus revealed the engineered C7 deletion and the two adaptive mutations (prM E21K and NS2B E27G) without any additional changes (Fig. S5b). The results indicate that the C7a/t virus is stable when propagated on the BHK-HA-C cells.

Minimal dose of C7a/t virus and neutralizing antibody titer required for protection against ZIKV infection in A129 mice

We evaluated the virulence and immunogenicity of C7a/t virus in A129 mice, defective in type-I interferon receptors (Rossi et al., 2016). Fig. 4a outlines the experimental design. Three-week-old mice were infected with 10^5 FFU of C7a/t or WT virus (strain FSS13025). The infected mice were evaluated for weight loss (Fig. 4b), viremia (Fig. 4c), and survival (Fig. 4d). Compared with the DPBS sham group, no weight loss was observed in the C7a/t virus-infected group, whereas the WT virus-infected animals exhibited a significant weight loss on day 7 and afterwards (Fig. 4b). The WT virus-infected mice developed robust viremia with a peak titer of 3×10^6 PFU/ml on day 3; in contrast, the C7a/t virus-infected mice did not produce any detectable viremia when assayed on BHK-HA-C cells (Fig. 4c). Neither morbidity nor mortality was observed in the C7a/t virus-infected mice, whereas 40% mortality was observed in the WT virus-infected animals (Fig. 4d). To increase the test sensitivity, we repeated the above experiment using RT-PCR to quantify the viral RNA levels in serum (RNAemia), brain, and testis from the C7a/t-infected mice. On day 3 post-immunization, 22% (n=2/9) of the C7a/t-infected animals displayed RNAemia that barely reached the detection limit of RT-PCR; all other mice exhibited undetectable RNAemia. On day 8 post-immunization, none of the animals yielded detectable RNAemia (Fig. S6a). No viral RNA was detected in the brain (Fig. S6b) or testis (Fig. S6c) on days 8 and 49 post-immunization, indicating no neuroinvasion or persistent infection. Collectively, the results demonstrate that the C7a/t virus is highly attenuated in A129 mice.

On day 28 post-vaccination, mice were bled (to measure neutralizing antibody titers) and subcutaneously challenged with 10^6 PFU of the epidemic ZIKV PRVABC59 strain. The C7a/t virus-immunized mice produced a neutralizing titer of 2.8×10^3 (the highest dilution folds of sera that reduced 50% of mCherry ZIKV infection on Vero cells), which was 2.3-fold lower than that of the WT virus-immunized mice (Fig. 4e). On days 2 and 3 post-challenge, no viremia was detected from the WT ZIKV-infected or C7a/t virus-vaccinated mice; in contrast, the DPBS-vaccinated mice produced high viremia (Fig. 4f). All mice survived after challenge, including the mock-vaccinated and challenged animals (data not shown); this is not surprising because these A129 mice were challenged at the age of seven-week old, which were too old to succumb to ZIKV infection (Rossi et al., 2016). To examine if ZIKV challenge boosted immune responses, we measured neutralizing activity on day 14 post-challenge. The C7a/t virus-vaccinated mice showed a 23-fold increase in neutralizing titers from 2.8×10^3 to 6.3×10^4 after challenge (Fig. 4e), demonstrating an anamnestic response and suggesting a low level of viral infection after challenge that was not detected

by plaque assay of serum. In contrast, the WT virus-infected mice did not boost neutralizing titers after challenge (Fig. 4e), suggesting a sterilizing immunity.

Using the same experimental scheme (Fig. 4a), we tested lower doses of C7a/t virus (10^3 and 10^4 FFU) and ultraviolet (UV)-inactivated C7a/t virus (10^5 FFU-equivalent) in A129 mice. Eighty percent (n=4/5) of the 10^4 FFU C7a/t-vaccinated animals seroconverted (Fig. S7a); two seroconverted animals with higher neutralizing antibody titers (280 and 1,016) were fully protected against viremia upon challenge, whereas the other two seroconverted animals with lower neutralizing antibody titers (108 and 123) generated viremia (Fig. S7b). None of the A129 mice vaccinated with 10^3 FFU C7a/t virus or DPBS seroconverted; only one mouse vaccinated with 10^5 FFU equivalent UV-inactivated C7a/t virus seroconverted with a low neutralizing antibody titer of 108 (Fig. S7a); all of these animals developed viremia after challenge (Fig. S7b). However, it is noticed that mice vaccinated with the UV-inactivated C7a/t virus exhibited significantly lower viremia than the DPBS- or 10^3 FFU C7a/t virus-vaccinated animals (Fig. S7b). A strong correlation (R^2=0.753) was observed between the levels of neutralizing titers and viremia ($p<0.0001$) (Fig. S7c, d). Seven out of 27 mice with neutralizing titers ≥280 were protected against viremia, all other mice with neutralizing titers ≤123 developed viremia after challenge (Fig. S7c). These results demonstrate that (i) a minimal dose of 10^5 FFU of C7a/t virus can confer 100% seroconversion and protection against viremia; (ii) a neutralizing antibody titer of ≥280 is sufficient for protection against viremia in A129 mice.

Protection from *in utero* transmission during pregnancy

We tested if vaccination with C7a/t virus could prevent *in utero* transmission during pregnancy. Fig. 5a outlines the experimental design. Three-week-old female mice were immunized with 10^5 FFU of C7a/t virus or DPBS sham. No viremia was detected on days 3 to 7 post-immunization (Fig. 5b). On day 28 post-immunization, the mice generated an average neutralizing antibody titer of 1.2×10^3 (Fig. 5c). The female mice were then mated with male mice during days 30 to 33 post-vaccination, and monitored for vaginal plugs when embryonic day 0.5 (E0.5) was defined. At E10.5, dams were bled (to measure neutralizing titers) and subcutaneously challenged with 10^6 PFU of ZIKV epidemic strain PRVABC59. At E10.5, the average neutralizing titer reached 3.8×10^3, 2-fold higher than that detected on day 28 post-immunization (Fig. 5c). At E12.5, no viremia was detected from the C7a/t virus-immunized animals, whereas a high viremia of 9×10^5 PFU/ml was detected from the DPBS-immunized mice (Fig. 5d). At E18.5, animals were sacrificed and measured for viral loads in maternal organs (brain, spleen, and placenta) and fetal heads. Infectious ZIKV was detected in 50% of the spleens (n=3/6) and 83% of the brains (n=5/6) from the DPBS-immunized group, but none (n=0/8) from the C7a/t virus-immunized group (Fig. 5e). High viral loads (average 8×10^5 PFU/g) were detected in every placenta (n=25/25) from the DPBS-immunized dams, whereas no infectious virus was detected in any placentas (n=0/36) from the C7a/t virus-immunized dams (Fig. 5f). Infectious virus (1×10^5 and 4×10^5 PFU/g) was detected in 8% of the fetal heads (n=2/25) from the DPBS group, whereas no infectious virus was detected in any fetal heads (n=0/36) from the C7a/t virus-immunized group (Fig. 5g). In addition, fetal weights from the C7a/t virus-immunized group were similar to those from the uninfected control group, whereas fetal weights were significantly lower in the

DPBS group (Fig. 5h). Interestingly, high neutralizing antibody titers of about 1.3×10^3 were detected in the fetal blood from the C7a/t virus-immunized group (Fig. 5i). Together, these results demonstrate that (i) vaccination with C7a/t virus can prevent maternal infection and *in utero* transmission of ZIKV during pregnancy, and (ii) maternal neutralizing antibodies (most likely IgGs, since IgM is not known to cross the placenta) can be transferred to fetuses from the immunized dams.

T cell response after C7a/t virus immunization in A129 mouse

T cell immunity plays an important role in preventing ZIKV infection (Elong Ngono et al., 2017). We analyzed the T cell responses in A129 mice subcutaneously inoculated with 10^5 FFU C7a/t viruses. Mouse spleens were harvested on days 8 and 49 post-immunization. Splenocytes were cultured *ex vivo*, stimulated with live ZIKV or a previously reported ZIKV E peptide (Elong Ngono et al., 2017), and analyzed by both an intracellular cytokine staining (ICS) assay and a Bio-Plex immunoassay. The C7a/t-immunized mice showed significantly more IFN-γ^+ and IFN-γ^+TNF-α^+ ZIKV-specific $CD4^+$ and $CD8^+$ T cells than the sham-vaccinated animals on days 8 (Fig. 6a, b and Fig. S8a-c) and 49 post-immunization (Fig. 6f, g and Fig. S8g-i). Consistently, the splenocytes from C7a/t-immunized mice produced significantly higher levels of interleukin-2 (IL-2), IFN-γ, and TNF-α than those from the sham group on days 8 (Fig. 6c-e and Fig. S8d-f) and 49 (Fig. 6h-j and Fig. S8j-l) post-immunization. These data indicate that the C7a/t immunization induces robust $CD4^+$ and $CD8^+$ T cell responses in mice.

Neurovirulence of C7a/t virus

To evaluate the neurovirulence of the C7a/t virus, we intracranially inoculated C7a/t virus into one-day-old CD-1 mice. We chose CD-1 mice because they have been used for neurovirulence analysis for other ZIKV LAV candidates (Shan et al., 2017a). In agreement with previous results (Shan et al., 2017b), 67% (n=6/9) of pups succumbed to 10^2 PFU of WT ZIKV FSS13025 infection. In contrast, no death was observed when neonates were injected with 10^4 PFU C7a/t virus or DPBS (Fig. S9). The results indicate that the C7a/t virus is highly attenuated in murine neurovirulence.

Discussion

Both LAVs (YFV 17D, JEV SA14–14-2, and Dengvaxia) and inactivated vaccines (JEV and TBEV) have been developed for flavivirus prevention in human use. A safe and efficacious ZIKV LAV is an attractive vaccine approach, particularly when the goal is to immunize general populations living in ZIKV-endemic areas. A number of ZIKV LAV candidates have been reported, including the 3'UTR deletion LAV (Shan et al., 2017a; Shan et al., 2017b), NS1 glycosylation knockout LAV (Richner et al., 2017a), E glycosylation knockout LAV (Fontes-Garfias et al., 2017), chimeric DENV-2 virus (Xie et al., 2017a), and chimeric JEV SA14–14-2 (Li et al., 2018b). Compared with these LAVs, our current C-deletion LAV has two major advantages.

First, the C-deletion LAV retains all ZIKV non-structural genes. Clinical studies of licensed YFV 17D and Dengvaxia suggest that T cell immunity is crucial for safe, efficacious, and

durable protection against flavivirus infection. Many T cell epitopes have been mapped to nonstructural proteins of flaviviruses, including ZIKV (Elong Ngono et al., 2017; Halstead, 2017; Lima et al., 2017; Rivino et al., 2013). Therefore, LAVs containing the authentic structural and non-structural proteins should elicit stronger viral specific $CD4^+$ and $CD8^+$ T cell responses than the chimeric flavivirus LAVs, inactivated vaccines, and subunit vaccines, all of which contain only the structural proteins of ZIKV. Although neutralizing antibodies have been recognized as correlates of protection against ZIKV and other flavivirus infections (Abbink et al., 2016; Abbink et al., 2017; Hombach et al., 2007; Hombach et al., 2005; Modjarrad et al., 2017), T cells play an essential role in mediating the quality and longevity of vaccine response. It is currently unknown if protection against *in utero* transmission of ZIKV during pregnancy requires both humoral and cellular immunity.

Second, the C-deletion LAV infects cells with limited, controlled infection rounds, representing an important safety feature, particularly when immunizing immunocompromised and pregnant individuals. Due to the presence of complete HA-C in virions, the C7a/t virus can launch one productive cycle of infection; during this single-round of replication, it generates prM/M-E empty particles and C7a virions (with nucleocapsid containing the C7 protein). Both the prM/M-E particles and C7a virions could elicit immune responses. However, the C7a virions cannot launch another round of replication after entry into cells, possibly due to defects in membrane fusion or nucleocapsid un-coating. Limited rounds of infection of C7a/t virus were observed in 7 out of 8 tested naïve cell lines. Only BHK-21 cells, from which the two adaptive viral mutations (prM E21K and NS2B E27G) were originally selected, could support multiple rounds of C7a/t viral infection. Future studies are needed to define the specific factor(s) in BHK-21 cells that accounts for the full infection cycle of C7a/t virus. We currently cannot exclude the possibility that other cell types are also able to support multiple rounds of C7a/t infection *in vivo*, which warrants future investigation. Given the subcutaneous route of administration, ZIKV-permissive cells around the injection site (*e.g.*, skin fibroblast, epidermal keratinocytes, and immature dendritic cells) may support restricted rounds of infection of C7a/t in mice (Hamel et al., 2015). Such limited rounds of infection (observed in cell culture) translated into an excellent safety profile *in vivo*. First, no viremia was detected (using focus-forming assay on BHK-HA-C cells) after vaccinating A129 mice with 10^5 FFU C7a/t virus. Second, no morbidity or mortality was observed in one-day-old CD-1 mice after intracranial infection with 10^4 FFU of C7a/t virus. Despite this excellent safety profile, a single-dose vaccination of C7a/t virus elicited a robust immune response and fully protected against ZIKV infection and *in utero* transmission in pregnant mice. Besides C-deletions, mutations in other genes that modulate viral assembly may also be utilized to develop safe and efficacious vaccines (Shan et al., 2018b).

It remains to be determined how the two adaptive mutations (prM E21K and NS2B E27G) enhance the *trans* complementation efficiency of C7a RNA on BHK-HA-C cells by ~100 fold. The genetic interaction between prM and C identified in this study is supported by the cryo-EM structure of the immature ZIKV showing that (i) a partially ordered C protein shell is located immediately below the base of the prM-E trimeric spikes and (ii) the prM E21K mutation is located at the interface between pr domains and are involved in the interactions within trimeric prM/E spikes (Prasad et al., 2017). NS2B of DENV and JEV is known to

modulate virion assembly (Li et al., 2016; Peng et al., 2018), supporting the role of NS2B E27G mutation in enhancing the production of C7a/t virus in the *trans* complementation system.

In summary, we developed a C-deletion ZIKV as a single-dose LAV with exceptional safety and immunogenicity. Our results suggest that further preclinical development of the Cdeletion LAV is warranted. The C-deletion ZIKV platform complements other promising vaccine platforms currently under development.

STAR Methods

Contact for Reagent and Resource Sharing

Further information and requests for resources and reagents should be directed to and will be fulfilled by Lead Contact, Dr. Pei-Yong Shi (peshi@utmb.edu)

Experimental Model and Subject Details

Cell Lines—The Baby hamster kidney fibroblast (BHK-21) cells, mouse myoblast (C2C12) cells, African green monkey kidney epithelial (Vero) cells, human brain glioblastoma cells (HTB-15) and human placenta epithelial cells (JEG-3) were purchased from the American Type Culture Collection (ATCC, Bethesda, MD) and maintained in a high-glucose Dulbecco's modified Eagle's medium (DMEM) supplemented with 10% fetal bovine serum (FBS) (HyClone Laboratories, South Logan, UT) and 1% penicillin/streptomycin (P/S). Human placenta trophoblast cells (HTR-8/SVneo) were purchased from ATCC and maintained in a RPMI medium with 5% FBS and 1% P/S. BHK-HA-C cells were grown in DMEM medium with additional 0.5 mg/ml Geneticin. Human alveolar basal epithelial cells (A549) were purchased from ATCC and cultured in DMEM supplemented with 10% FBS, 1% P/S and 1% HEPES. All cells were cultured at 37°C with 5% CO_2. All culture medium, NEAA, HEPES and antibiotics were purchased from ThermoFisher Scientific (Waltham, MA).

Animals—CD-1® IGS outbred mice were purchased from Charles River Laboratories (Wilmington, MA). A129 mice (*Ifnar1*^{tm1Agt}, IFN type I receptor knockout) were purchased from Jackson laboratories (Bar Harbor, ME). Both mice were housed in specific pathogen-free conditions in the Animal Resource Center at the University of Texas Medical Branch (UTMB; Galveston, TX). For neurovirulence studies, pregnant CD-1® IGS females were housed individually in microisolator cages. One day after delivery, neonates were used for intracranial injection. After injection, neonates were housed together with corresponding dams. Three-week old A129 mice (about 50% females and males) were used for vaccination studies. Female and male A129 mice were separated and housed in microisolator cages at no more than 5 mice/cage. For pregnancy studies, an individual male (2–3-month old) and female (7-week old) were introduced to the same cage for mating. At the time vaginal plug was confirmed, the females were separated into microisolator cages. Animals had access to water and food *ad libitum*. All animal procedures were performed as approved by the University of Texas Medical Branch (UTMB) Institutional Animal Care and Use Committee (IACUC).

Method Details

Antibodies—The following antibodies were used in this study: mouse monoclonal antibody (mAb) 4G2 (which is cross-reactive with flavivirus E protein) produced from a mouse hybridoma cell line D1–4G2–4-15 (ATCC), rabbit anti-ZIKV prM (Alpha Diagnostic Intl Inc., San Antonio, TX), anti-ZIKV E and NS3 antibodies (GeneTex, Irvine, CA), mouse polyclonal antibody against ZIKV NS1 (in-house generated using the recombinant ZIKV NS1 antigen purified from *E.coli*.), rabbit anti-HA antibody (Abcam, Cambridge, MA), mouse polyclonal antibody against ZIKV capsid (inhouse generated using the recombinant ZIKV capsid antigen purified from *E.coli*.), ZIKV-specific HMAF (hyper-immune ascitic fluid; obtained from the World Reference Center of Emerging Viruses and Arboviruses [WRCEVA] at the University of Texas Medical Branch), goat antimouse or anti-rabbit IgGs conjugated with horseradish peroxidase (HRP) purchased from KPL (Gaithersburg, MD) and Sigma-Aldrich (St. Louis, MO), and goat anti-mouse IgGs conjugated with Alexa 488 (Thermo Fisher Scientific). Antibodies used for intracellular cytokine staining (see description below) were purchased from Thermo Fisher Scientific.

Plasmid Construction—The ZIKV full-length cDNA infectious clone pFLZIKV (Shan et al., 2016b) was used as the backbone for engineering capsid deletion mutants. Standard overlap PCR was performed to amplify the DNA fragment between unique restriction enzyme sites NotI and AvrII that contained the corresponding capsid deletion mutants. Afterwards, the fragments were cloned into the infectious clone pFLZIKV through NotI and AvrII sites. Two unique restriction sites ApaLI and KasI were used to engineer the NS2B E27G mutation into pFLZIKV or C7 clone. Plasmids were propagated in *E. coli* strain Top 10 (ThermoFisher Scientific). All restriction enzymes were purchased from New England BioLabs (Ipswitch, MA). The plasmids were validated by restriction enzyme digestion and Sanger DNA sequencing. All primers were synthesized from Integrated DNA Technologies (Skokie, Illinois) and are available upon request.

RNA Transcription and Electroporation—Plasmids were linearized by restriction enzyme ClaI. RNA transcription and electroporation were performed as described previously (Shan et al., 2016b). Briefly, 10 μg RNA was electroporated into 8×10^6 cells in a 4-mm cuvette using the GenePulser apparatus (Bio-Rad) at settings of 0.45 kV (Vero cells) or 0.85 kV (BHK-21 and BHK-HA-C cells) and 25 mF, pulsing three times, with 3 s intervals. After a 10-min recovery at room temperature, transfected cells were suspended in culture media and incubated at 37°C wi th 5% CO_2.

Immunofluorescence assay (IFA)—Cells were seeded in an 8-well Lab-Tek II chamber slide (Thermo Fisher Scientific). At given time points, cells were fixed in 100% methanol at −20°C for 15 min. After 1 h incubation in blocking buffer containing 1% FBS and 0.05% Tween-20 in PBS, cells were treated with primary antibodies for 1 h and washed three times with PBS (5 min per wash). Cells were then incubated with goat anti-mouse or rabbit IgG conjugated with Alexa Fluor 488 (Thermo Fisher Scientific) for 1 h in blocking buffer. After three PBS-washes, cells were mounted in a Vectashield mounting medium with DAPI (Vector Laboratories). Fluorescence images were acquired under Eclipse Ti2 inverted fluorescence microscope (Nikon Instruments Inc.).

SDS-PAGE and Western Blot—After transfection, culture medium was clarified by centrifuging at 500×g for 5 min to remove cell debris. Supernatants were collected and mixed with 4×LDS sample buffer (Thermo Fisher Scientific). After denaturing at 70°C for 15 min, 3 0 μl samples were loaded onto to a 12% or 15% SDS-PAGE gel (Bio-Rad Laboratories). After electrophoresis, proteins were resolved and transferred onto a polyvinylidene difluoride (PVDF) membrane using the Bio-Rad TransBlot Turbo Blotting System. Blots were soaked for 1 hour in a blocking buffer containing TBST (10 mM Tris-HCl [pH 7.5], 150 mM NaCl, and 0.1% Tween 20) and 5% skim milk, followed by 1 h incubation with primary antibodies (1:1,000 diluted in blocking buffer). After three washes with TBST buffer, blots were incubated with goat anti-mouse or rabbit antibodies conjugated to HRP (1:10,000 diluted in blocking buffer. After three thorough washes with TBST buffer, blots were incubated with SuperSignal™ West Femto Maximum Sensitivity Substrate (Thermo Fisher Scientific). Chemiluminescence signals were detected in ChemiDoc System (Bio-Rad).

Focus-forming assay and Immunostaining—Focus-forming assay and immunostaining was performed to determine the amount of infectious viruses in the culture medium and mouse sera. 2×10^5 Vero, BHK-21 or BHK-HA-C cells per well were seeded in 24-well plates. At 16–20 h post-seeding, 100 μl virus samples (serial tenfold dilutions: 10^1-10^6 in DMEM) were prepared and inoculated into each well of 24-well plates with 100% cell confluence. After incubation at 37°C for 1 h, the inoculum was replaced with 0.6 ml of overlay medium containing 0.8% methylcellulose. Plates were incubated at 37°C for 5 days. Afterwards, immunostaining was performed as described previously (Shan et al., 2017b).

Virus replication Kinetics—Cells (8×10^5 cells/well) were seeded in a 6-well plate. One day after seeding, cells were infected with WT or mutant ZIKV at an MOI of 0.1–0.5. Infection was performed in triplicates at 37°C. After 1 h of infection, inoculums were removed and cells were washed extensively with PBS to eliminate unbound viruses. Afterwards, 3 ml of fresh medium was added to each well. From day 1 to 4 post-infection, 200 μl of supernatants was collected daily and clarified by centrifugation at 500×g for 5 min prior to storage at −80°C. Virus ti ters in the culture fluids were determined by focus-forming assay.

RNA extraction and qRT-PCR—At given time points, culture fluids were harvested and clarified by centrifugation at 500×g for 5 min. Culture fluids (140 μl) were used for extracellular viral RNA extraction by QIAamp viral RNA mini kit (Qiagen). After infection or electroporation, cells from 6-well plates were washed thoroughly with PBS. Intracellular RNAs were isolated using an RNeasy mini kit (Qiagen). Quantitative reverse transcription PCR (qRT-PCR) assays were performed using the QuantiTect Probe RT-PCR kit (Qiagen) or iScript SYBR Green One-Step kit (BioRad) in a LightCycler 480 system (Roche, Basel, Switzerland) following the manufacturer's protocols. Primers ZIKV-6878V (5'-CATGGTAGCAGTGGGTCTTC-3'), ZIKV-6980R (5'-CTCCTCTCTCCTTCCCATTAGA-3') and probe ZIKV-6908-FAM (5'-FAM/TA CCG CCA

A/ZEN/T GAA CTC GGA TGG TT/3IABkFQ-3') were used in this study. Detailed procedures were described before (Yang et al., 2017).

Selection of stable BHK-HA-C cell line—The plasmid pXJ-HA-C (containing a neomycin resistance gene) was used for establishing cell lines constitutively expressing HA-C fusion protein. The HA-C gene cassette was amplified by overlap PCR and cloned into a pXJ vector (Xie et al., 2015) using NotI and XhoI restriction enzyme sites. About 1×10^5 BHK-21 cells per well in a 6-well plate were transfected with 1 μg of plasmids using the X-tremeGENE 9 DNA transfection reagent (Roche, Basel, Switzerland). At 24 h post-transfection, G418 (ThermoFisher Scientific) was added to a final concentration of 1 mg/ml. The culture medium was replaced with fresh medium containing 1 mg/ml G418 every three days. After about 2 weeks, G418-resistant colonies were formed, harvested and further expanded. Cells were characterized by fluorescence microscopy using rabbit anti-HA antibodies.

ZIKV/mcherry Neutralization Assay—Titers of neutralizing antibody in mouse serum were determined by using an mCherry ZIKV infection assay as described previously (Shan et al., 2017b). Briefly, sera were 2-fold serially diluted (starting at 1:25 dilution) in culture medium and then incubated with equal volume of ZIKV/mCherry reporter viruses at 37°C for 1 h. Afte rwards, antibody-virus complexes were added to Vero cell monolayers in a 96-well plate. At 48 h post-infection, mCherry fluorescencepositive cells were quantified by the Cytation 5 Cell Imaging Multi-Mode Reader (Biotek). Fluorescence-positive cells from serum-treated wells were normalized to those of non-treatment controls (set as 100%). The effective dilution of sera to reduce percentage of mCherry-positive cells by 50% (NT_{50}) was calculated using nonlinear regression analysis in GraphPad Prism 7 software (La Jolla, CA).

Mouse Experiments—Virulence and immunogenicity of vaccine candidates were evaluated using 3-week-old A129 mice (a model susceptible to ZIKV infection) (Rossi et al., 2016). A129 mice were subcutaneously injected with 100 μl WT or mutant virus with desired concentrations. Mockinfected mice were given DPBS by the same route. Mice were monitored for weight loss and signs of disease daily. At given time points, mice were bled via the retro-orbital sinus (RO) and viremia was determined by plaque assay on BHK-HA-C cells. On day 28 post-immunization, mice were bled and neutralizing antibodies were measured using ZIKV/mCherry infection assay. Mice were challenged on day 28 post-immunization with parental ZIKV strain PRVABC59 (10^6 PFU) via subcutaneous injection. On day 2 post-challenge, mice were bled and viremia was determined by plaque assay on Vero cells.

For the mouse pregnancy study, immunization was done according to the same procedure as described above. On day 28 p.i., mice were bled to measure NT_{50}. Mice were mated starting on day 30 post-immunization. Mouse embryonic development started (E0.5) once mouse vaginal plugs were observed. At E10.5, mice were bled to quantify neutralizing antibodies, and immediately challenged with parental ZIKV strain PRVABC59 (10^6 PFU) via subcutaneous injection. Two days after challenge, mice were bled to measure viremia. At E18.5, all dams were euthanized and maternal tissues (brain, spleen and placenta) and fetus were harvested. Fetal weight was measured immediately. After decapitation, fetal heads and

blood were collected. Tissues were homogenized in 500 μl of DMEM medium using the TissueLyser II (Qiagen) for 5 min at 30 Hz. After centrifugation at 15000×rpm for 10 min, supernatants were harvested. Plaque assays were performed on Vero cells to determine virus loads in maternal brain, spleen and placenta and fetal head. Neutralizing antibodies in fetal blood were measured using ZIKV/mCherry infection assay as described above.

Intracellular cytokine staining (ICS)—Approximately 2.5×10^6 splenocytes were stimulated with 1×10^5 IFU live ZIKV (strain FSS13025) for 24 h or 10 μg/ml E peptide (Sequence 294–302 in ZIKV polyprotein) (Elong Ngono et al., 2017) for 5 h. Live ZIKV was used as a stimulant to measure both $CD4^+$ and $CD8^+$ T cell response (Shan et al., 2017b). The E peptide was used as a stimulant to measure $CD8^+$ T cell response (Elong Ngono et al., 2017). During the final 5 h of stimulation, BD GolgiPlug (BD Bioscience) was added to block protein transport. Cells were stained with antibodies for CD3 (APC-conjugated), CD4 (FITC-conjugated), or CD8 (FITC-conjugated). Afterwards, cells were fixed in 2% paraformaldehyde and permeabilized with 0.5% saponin. Cells were then incubated with PE-conjugated anti-IFN-γ and PE-Cy7-conjugated anti-TNF-α antibodies or control PEconjugated rat IgG1. Samples were processed with a BD Accuri™ C6 Flow Cytometer instrument. Dead cells were excluded on the basis of forward and side light scatter. Data were analyzed with a CFlow Plus Flow Cytometer (BD Biosciences).

Bio-Plex immunoassay—Approximately 3×10^5 splenocytes were plated in 96-well plates and stimulated with 2×10^4 FFU ZIKV strain FSS13025 for 2 days or 10 μg/ml E peptide for 3 days, respectively. Culture supernatants were harvested and frozen at −80°C. Cytokines IL-2, IFN-Y and TNF-α in the culture supernatants were measured using a Bio-Plex Pro Mouse Cytokine Assay (Bio-Rad, Hercules, CA) according to the manufacturer's instructions.

Neurovirulence in Newborn CD-1 Mice—Groups of 1-day-old outbred CD-1 neonates (n=8 to 9) were intracranially injected with WT ZIKV strain FSS13025 (100 PFU) or mutant viruses (10,000 FFU). Mice were monitored daily for morbidity and mortality over 20 days.

Quantification and Statistical Analysis

The amino acid alignment was performed with default settings using the CLC main workbench software (Qiagen). IFA images processing and cell counting was performed in software ImageJ (NIH). At least three different IFA images were used to estimate the mean and standard deviations of percentage of viral protein staining positive-cells in Figure 1e and 3f-g. Densitometry analysis was performed using Image lab version 6.0 (Bio-Rad Laboratories, Hercules, CA). All numerical data are presented as the mean ± SEM (standard error of mean).

Group comparisons were performed using multiple t-tests, unpaired nonparametric Mann-Whitney unpaired test or two-way ANOVA with a multiple comparisons correction in GraphPad Prism 7.0 software. Log-rank (Mantel-Cox) test was performed for analyzing statistical significance of survival. *$p<0.05$, significant; **$p<0.01$, very significant; ***$p<0.001$, highly significant; ****$p<0.0001$, extremely significant; n.s., not significant.

The size of each study or number of replicates, along with the statistical tests performed can be found in corresponding Figure Legends.

Supplementary Material

Refer to Web version on PubMed Central for supplementary material.

Acknowledgements

We thank Maki Wakamiya, Jiaren Sun, Yuejin Liang, W. Sam Fagg, Shelton Bradrick, Mariano Garcia-Blanco, and other colleagues at University of Texas Medical Branch for helpful discussions and support. P.-Y.S. lab was supported by a Kleberg Foundation Award and NIH grant AI127744. This research was also partially supported by NIH grant AI120942 to S.C.W. and by Cooperative Agreement Number U01CK000512 to S.C.W., funded by the CDC.

References

Abbink P, Larocca RA, De La Barrera RA, Bricault CA, Moseley ET, Boyd M, Kirilova M, Li Z, Ng'ang'a D, Nanayakkara O, et al. (2016). Protective efficacy of multiple vaccine platforms against Zika virus challenge in rhesus monkeys. Science 353, 1129–1132. [PubMed: 27492477]

Abbink P, Larocca RA, Visitsunthorn K, Boyd M, De La Barrera RA, Gromowski GD, Kirilova M, Peterson R, Li Z, Nanayakkara O, et al. (2017). Durability and correlates of vaccine protection against Zika virus in rhesus monkeys. Sci Transl Med 9.

Aliota MT, Bassit L, Bradrick SS, Cox B, Garcia-Blanco MA, Gavegnano C, Friedrich TC, Golos TG, Griffin DE, Haddow A, et al. (2017). Zika in the Americas, year 2: What have we learned? What gaps remain? A report from the Global Virus Network. Antiviral Res.

Betancourt D, de Queiroz NM, Xia T, Ahn J, and Barber GN (2017). Cutting Edge: Innate Immune Augmenting Vesicular Stomatitis Virus Expressing Zika Virus Proteins Confers Protective Immunity. J Immunol 198, 3023–3028. [PubMed: 28289159]

Brasil P, Pereira JP, Jr., Moreira ME, Ribeiro Nogueira RM, Damasceno L, Wakimoto M, Rabello RS, Valderramos SG, Halai UA, Salles TS, et al. (2016). Zika Virus Infection in Pregnant Women in Rio de Janeiro. N Engl J Med 375, 2321–2334. [PubMed: 26943629]

Cao-Lormeau VM, Blake A, Mons S, Lastere S, Roche C, Vanhomwegen J, Dub T, Baudouin L, Teissier A, Larre P, et al. (2016). Guillain-Barre Syndrome outbreak associated with Zika virus infection in French Polynesia: a case-control study. Lancet 387, 1531–1539. [PubMed: 26948433]

Chang DC, Liu WJ, Anraku I, Clark DC, Pollitt CC, Suhrbier A, Hall RA, and Khromykh AA (2008). Single-round infectious particles enhance immunogenicity of a DNA vaccine against West Nile virus. Nat Biotechnol 26, 571–577. [PubMed: 18425125]

Dokland T, Walsh M, Mackenzie JM, Khromykh AA, Ee KH, and Wang S (2004). West Nile virus core protein; tetramer structure and ribbon formation. Structure 12, 1157–1163. [PubMed: 15242592]

Dowd KA, Ko SY, Morabito KM, Yang ES, Pelc RS, DeMaso CR, Castilho LR, Abbink P, Boyd M, Nityanandam R, et al. (2016). Rapid development of a DNA vaccine for Zika virus. Science 354, 237–240. [PubMed: 27708058]

Elong Ngono A, Vizcarra EA, Tang WW, Sheets N, Joo Y, Kim K, Gorman MJ, Diamond MS, and Shresta S (2017). Mapping and Role of the CD8(+) T Cell Response During Primary Zika Virus Infection in Mice. Cell Host Microbe 21, 35–46. [PubMed: 28081442]

Fontes-Garfias CR, Shan C, Luo H, Muruato AE, Medeiros DBA, Mays E, Xie X, Zou J, Roundy CM, Wakamiya M, et al. (2017). Functional Analysis of Glycosylation of Zika Virus Envelope Protein. Cell Rep 21, 1180–1190. [PubMed: 29091758]

Gaudinski MR, Houser KV, Morabito KM, Hu Z, Yamshchikov G, Rothwell RS, Berkowitz N, Mendoza F, Saunders JG, Novik L, et al. (2017). Safety, tolerability, and immunogenicity of two Zika virus DNA vaccine candidates in healthy adults: randomised, open-label, phase 1 clinical

trials. Lancet. Halstead, S.B. (2017). Achieving safe, effective, and durable Zika virus vaccines: lessons from dengue. The Lancet Infectious diseases 17, e378–e382. [PubMed: 28711586]

Hamel R, Dejarnac O, Wichit S, Ekchariyawat P, Neyret A, Luplertlop N, Perera-Lecoin M, Surasombatpattana P, Talignani L, Thomas F, et al. (2015). Biology of Zika Virus Infection in Human Skin Cells. J Virol 89, 8880–8896. [PubMed: 26085147]

Hombach J, Cardosa MJ, Sabchareon A, Vaughn DW, and Barrett AD (2007). Scientific consultation on immunological correlates of protection induced by dengue vaccines report from a meeting held at the World Health Organization 17–18 November 2005. Vaccine 25, 4130–4139. [PubMed: 17428588]

Hombach J, Solomon T, Kurane I, Jacobson J, and Wood D (2005). Report on a WHO consultation on immunological endpoints for evaluation of new Japanese encephalitis vaccines, WHO, Geneva, 2–3 September, 2004. Vaccine 23, 5205–5211. [PubMed: 16055233]

Kofler R, Heinz F, and Mandl C (2002). Capsid protein C of tick-borne encephalitis virus tolerates large internal deletions and is a favorable target for attenuation of virulence. J Virol 76, 3534–3543. [PubMed: 11884577]

Kofler RM, Aberle JH, Aberle SW, Allison SL, Heinz FX, and Mandl CW (2004). Mimicking live flavivirus immunization with a noninfectious RNA vaccine. Proc Natl Acad Sci U S A 101, 1951–1956. [PubMed: 14769933]

Larocca RA, Abbink P, Peron JP, Zanotto PM, Iampietro MJ, Badamchi-Zadeh A, Boyd M, Ng'ang'a D, Kirilova M, Nityanandam R, et al. (2016). Vaccine protection against Zika virus from Brazil. Nature 536, 474–478. [PubMed: 27355570]

Li T, Zhao Q, Yang X, Chen C, Yang K, Wu C, Zhang T, Duan Y, Xue X, Mi K, et al. (2018a). Structural insight into the Zika virus capsid encapsulating the viral genome. Cell Res 28, 497–499. [PubMed: 29467384]

Li XD, Deng CL, Ye HQ, Zhang HL, Zhang QY, Chen DD, Zhang PT, Shi PY, Yuan ZM, and Zhang B (2016). Transmembrane Domains of NS2B Contribute to both Viral RNA Replication and Particle Formation in Japanese Encephalitis Virus. J Virol 90, 5735–5749. [PubMed: 27053551]

Li XF, Dong HL, Wang HJ, Huang XY, Qiu YF, Ji X, Ye Q, Li C, Liu Y, Deng YQ, et al. (2018b). Development of a chimeric Zika vaccine using a licensed live-attenuated flavivirus vaccine as backbone. Nat Commun 9, 673. [PubMed: 29445153]

Lima NS, Rolland M, Modjarrad K, and Trautmann L (2017). T Cell Immunity and Zika Virus Vaccine Development. Trends in immunology 38, 594–605. [PubMed: 28579320]

Liu Y, Liu J, Du S, Shan C, Nie K, Zhang R, Li XF, Zhang R, Wang T, Qin CF, et al. (2017). Evolutionary enhancement of Zika virus infectivity in Aedes aegypti mosquitoes. Nature 545, 482–486. [PubMed: 28514450]

Ma L, Jones CT, Groesch TD, Kuhn RJ, and Post CB (2004). Solution structure of dengue virus capsid protein reveals another fold. Proc Natl Acad Sci U S A 101, 3414–3419. [PubMed: 14993605]

Modjarrad K, Lin L, George SL, Stephenson KE, Eckels KH, De La Barrera RA, Jarman RG, Sondergaard E, Tennant J, Ansel JL, et al. (2017). Preliminary aggregate safety and immunogenicity results from three trials of a purified inactivated Zika virus vaccine candidate: phase 1, randomised, double-blind, placebo-controlled clinical trials. Lancet.

Pardi N, Hogan MJ, Pelc RS, Muramatsu H, Andersen H, DeMaso CR, Dowd KA, Sutherland LL, Scearce RM, Parks R, et al. (2017). Zika virus protection by a single low-dose nucleoside-modified mRNA vaccination. Nature.

Patkar CG, Jones CT, Chang YH, Warrier R, and Kuhn RJ (2007). Functional requirements of the yellow fever virus capsid protein. J Virol 81, 6471–6481. [PubMed: 17526891]

Peng M, Swarbrick CMD, Chan KW, Luo D, Zhang W, Lai X, Li G, and Vasudevan SG (2018). Luteolin escape mutants of dengue virus map to prM and NS2B and reveal viral plasticity during maturation. Antiviral Res 154, 87–96. [PubMed: 29665375]

Pierson TC, and Diamond MS (2013). Flaviviruses p 747–794 In Knipe DM and Howley PM (ed), Fields virology, 6th, vol 1.

Prasad VM, Miller AS, Klose T, Sirohi D, Buda G, Jiang W, Kuhn RJ, and Rossmann MG (2017). Structure of the immature Zika virus at 9 A resolution. Nat Struct Mol Biol 24, 184–186. [PubMed: 28067914]

Rasmussen SA, Jamieson DJ, Honein MA, and Petersen LR (2016). Zika Virus and Birth Defects - Reviewing the Evidence for Causality. N Engl J Med.

Richner J, Jagger B, Shan C, Fontes C, Dowd K, Cao B, Himansu S, Caine E, Nunes B, Medeiros D, et al. (2017a). Vaccine mediated protection against Zika virus induced congenital disease. Cell 170, 273–283. [PubMed: 28708997]

Richner JM, Himansu S, Dowd KA, Butler SL, Salazar V, Fox JM, Julander JG, Tang WW, Shresta S, Pierson TC, et al. (2017b). Modified mRNA Vaccines Protect against Zika Virus Infection. Cell.

Rivino L, Kumaran EA, Jovanovic V, Nadua K, Teo EW, Pang SW, Teo GH, Gan VC, Lye DC, Leo YS, et al. (2013). Differential targeting of viral components by CD4+ versus CD8+ T lymphocytes in dengue virus infection. J Virol 87, 2693–2706. [PubMed: 23255803]

Rossi SL, Tesh RB, Azar SR, Muruato AE, Hanley KA, Auguste AJ, Langsjoen RM, Paessler S, Vasilakis N, and Weaver SC (2016). Characterization of a Novel Murine Model to Study Zika Virus. Am J Trop Med Hyg 94, 1362–1369. [PubMed: 27022155]

Schlick P, Kofler RM, Schittl B, Taucher C, Nagy E, Meinke A, and Mandl CW (2010). Characterization of West Nile virus live vaccine candidates attenuated by capsid deletion mutations. Vaccine 28, 5903–5909. [PubMed: 20600500]

Schlick P, Taucher C, Schittl B, Tran JL, Kofler RM, Schueler W, von Gabain A, Meinke A, and Mandl CW (2009). Helices alpha2 and alpha3 of West Nile virus capsid protein are dispensable for assembly of infectious virions. J Virol 83, 5581–5591. [PubMed: 19297470]

Shan C, Muruato AE, Jagger BW, Richner J, Nunes BTD, Medeiros DBA, Xie X, Nunes JGC, Morabito KM, Kong WP, et al. (2017a). A single-dose live-attenuated vaccine prevents Zika virus pregnancy transmission and testis damage. Nat Commun 8, 676. [PubMed: 28939807]

Shan C, Muruato AE, Nunes BTD, Luo H, Xie X, Medeiros DBA, Wakamiya M, Tesh RB, Barrett AD, Wang T, et al. (2017b). A live-attenuated Zika virus vaccine candidate induces sterilizing immunity in mouse models. Nat Med 23, 763–767. [PubMed: 28394328]

Shan C, Xie X, Barrett ADT, Garcia-Blanco MA, Tesh RB, Vasconcelos PFC, Vasilakis N, Weaver SC, and Shi PY (2016a). Zika Virus: Diagnosis, Therapeutics, and Vaccine ACS Infectious Diseases 2, 170–172. [PubMed: 27623030]

Shan C, Xie X, Muruato AE, Rossi SL, Roundy CM, Azar SR, Yang Y, Tesh RB, Bourne N, Barrett AD, et al. (2016b). An Infectious cDNA Clone of Zika Virus to Study Viral Virulence, Mosquito Transmission, and Antiviral Inhibitors. Cell Host Microbe 19, 891–900. [PubMed: 27198478]

Shan C, Xie X, and Shi PY (2018a). Zika Virus Vaccine: Progress and Challenges. Cell Host Microbe 24, 12–17. [PubMed: 30008291]

Shan C, Xie X, Zou J, Zust R, Zhang B, Ambrose R, Mackenzie J, Fink K, and Shi PY (2018b). Using a virion assembly-defective dengue virus as a vaccine approach. J Virol.

Shang Z, Song H, Shi Y, Qi J, and Gao GF (2018). Crystal Structure of the Capsid Protein from Zika Virus. J Mol Biol 430, 948–962. [PubMed: 29454707]

Tebas P, Roberts CC, Muthumani K, Reuschel EL, Kudchodkar SB, Zaidi FI, White S, Khan AS, Racine T, Choi H, et al. (2017). Safety and Immunogenicity of an Anti-Zika Virus DNA Vaccine - Preliminary Report. N Engl J Med.

Widman DG, Ishikawa T, Fayzulin R, Bourne N, and Mason PW (2008). Construction and characterization of a second-generation pseudoinfectious West Nile virus vaccine propagated using a new cultivation system. Vaccine 26, 2762–2771. [PubMed: 18423946]

Widman DG, Ishikawa T, Winkelmann ER, Infante E, Bourne N, and Mason PW (2009). RepliVAX WN, a single-cycle flavivirus vaccine to prevent West Nile disease, elicits durable protective immunity in hamsters. Vaccine 27, 5550–5553. [PubMed: 19635608]

Xia H, Luo H, Shan C, Muruato AE, Nunes BTD, Medeiros DBA, Zou J, Xie X, Giraldo MI, Vasconcelos PFC, et al. (2018). An evolutionary NS1 mutation enhances Zika virus evasion of host interferon induction. Nat Comm In press.

Xie X, Yang Y, Muruato AE, Zou J, Shan C, Nunes BT, Medeiros DB, Vasconcelos PF, Weaver SC, Rossi SL, et al. (2017a). Understanding Zika Virus Stability and Developing a Chimeric Vaccine through Functional Analysis. MBio 8.

Xie X, Zou J, Puttikhunt C, Yuan Z, and Shi PY (2015). Two distinct sets of NS2A molecules are responsible for dengue virus RNA synthesis and virion assembly. J Virol 89, 1298–1313. [PubMed: 25392211]

Xie X, Zou J, Shan C, and Shi PY (2017b). Small Molecules and Antibodies for Zika Therapy. J Infect Dis 216, S945–S950. [PubMed: 29267911]

Yang Y, Shan C, Zou J, Muruato AE, Bruno DN, de Almeida Medeiros Daniele B, Vasconcelos PFC, Rossi SL, Weaver SC, Xie X, et al. (2017). A cDNA Clone-Launched Platform for High-Yield Production of Inactivated Zika Vaccine. EBioMedicine 17, 145–156. [PubMed: 28196656]

Yuan L, Huang XY, Liu ZY, Zhang F, Zhu XL, Yu JY, Ji X, Xu YP, Li G, Li C, et al. (2017). A single mutation in the prM protein of Zika virus contributes to fetal microcephaly. Science 358, 933–936. [PubMed: 28971967]

Zhu W, Qin C, Chen S, Jiang T, Yu M, Yu X, and Qin E (2007). Attenuated dengue 2 viruses with deletions in capsid protein derived from an infectious full-length cDNA clone. Virus Res 126, 226–232. [PubMed: 17412442]

Highlights

- A 9-residue capsid protein deletion (C7) limits ZIKV infection to one to two rounds
- Single-dose immunization of mice with C7 elicits robust protective responses to ZIKV
- Single vaccination with C7 prevents vertical transmission of ZIKV in pregnant mice
- Intracranial injection of C7 to neonates did not cause any disease or death

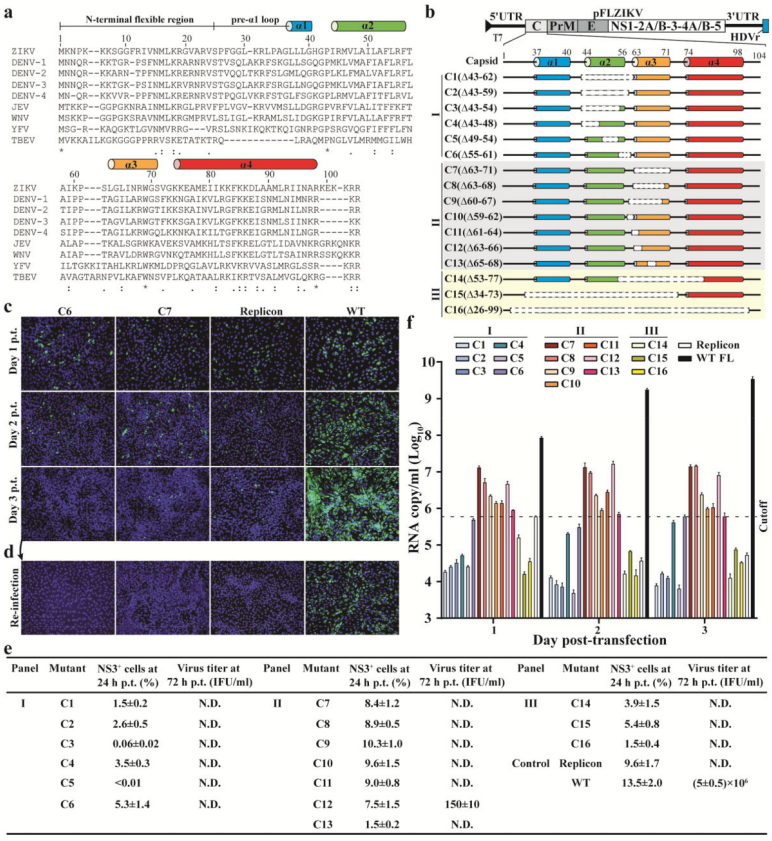

e

Panel	Mutant	NS3⁺ cells at 24 h p.t. (%)	Virus titer at 72 h p.t. (IFU/ml)	Panel	Mutant	NS3⁺ cells at 24 h p.t. (%)	Virus titer at 72 h p.t. (IFU/ml)	Panel	Mutant	NS3⁺ cells at 24 h p.t. (%)	Virus titer at 72 h p.t. (IFU/ml)
I	C1	1.5±0.2	N.D.	II	C7	8.4±1.2	N.D.	III	C14	3.9±1.5	N.D.
	C2	2.6±0.5	N.D.		C8	8.9±0.5	N.D.		C15	5.4±0.8	N.D.
	C3	0.06±0.02	N.D.		C9	10.3±1.0	N.D.		C16	1.5±0.4	N.D.
	C4	3.5±0.3	N.D.		C10	9.6±1.5	N.D.	Control	Replicon	9.6±1.7	N.D.
	C5	<0.01	N.D.		C11	9.0±0.8	N.D.		WT	13.5±2.0	(5±0.5)×10⁶
	C6	5.3±1.4	N.D.		C12	7.5±1.5	150±10				
					C13	1.5±0.2	N.D.				

Figure 1.

Characterization of C-deletion mutants. (a) Sequence alignment of flavivirus C protein. The alignment was performed using the CLC main workbench software (Qiagen). The structural features of ZIKV C protein are indicated. Below are the virus strains with the corresponding GenBank access numbers: ZIKV strain FSS13025 (KU955593), DENV-2 strain New Guinea C (AF038403), DENV-1 strain Westpac (U88535), DENV-3 strain H87 (M93130), DENV-4 strain H241 (AY947539), JEV strain SA14–14-2 (JN604986), WNV strain NY99 (AF196835), YFV strain 17D (JX949181), and TBEV strain A104 (KF151173). (b) Diagram of C-deletion mutants in the context of ZIKV genome. Dashed boxes indicate the deleted segments. Amino acid positions are indicated. (c) Immunofluorescent assay (IFA) of RNA-transfected Vero cells. At given time points post-transfection, Vero cells were fixed and stained with NS3 antibody for viral protein expression (green). Nuclei were counterstained by DAPI (blue). (d) IFA of infected Vero cells. Naive Vero cells were infected with the supernatant that was harvested from the RNAtransfected cells at 72 h post-transfection. At 24 h p.i., cells were analyzed by IFA for viral NS3 expression. (e) Summary of C-deletion mutants after transfecting viral RNA into Vero cells. Percentages of NS3-expressing cells ($NS3^+$) were calculated as follow: ($NS3^+$ cell number) / ($DAPI^+$ cell number)×100%. Supernatants at 72 h p.t. were used to infect naive Vero monolayers in 8-well chamber slides. At 24 h p.i., cells were fixed and monitored for NS3 expression by IFA. $NS3^+$ cells were counted and the virus titers (IFU/ml) were calculated. Limit of detection, 10 IFU/ml; N.D., not detectable. (f) Amounts of extracellular viral RNA post-transfection. At indicated time points, viral RNA levels in supernatant were quantified by RT-PCR. The

maximum amount of extracellular viral RNA from replicon RNA-transfected cells was set as the cutoff.

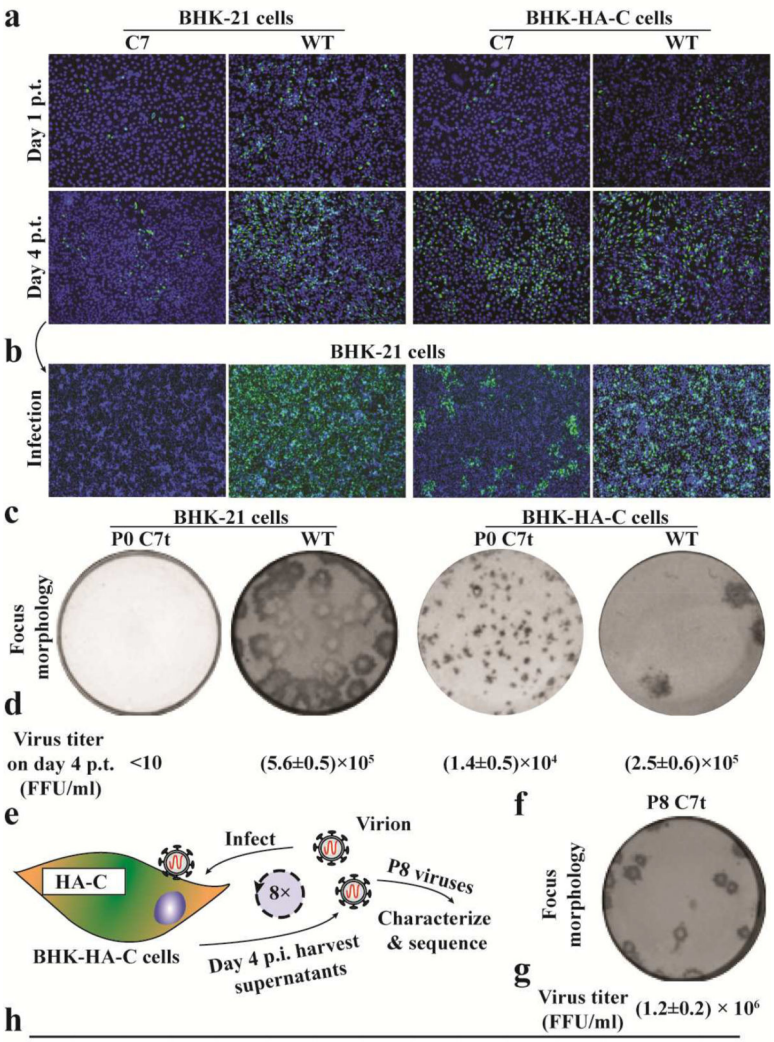

h

Mutant	Nucleotide change	Amino acid change and location
P8 C7t	294-320 deletion	63-71 deletion, Capsid
	G534A	E21K, PrM
	A4303G	E27G, NS2B
	G8516A	E283E (silent), NS5

Figure 2.

Trans complementation of the C7 mutant. (a) IFA after transfection. BHK-21 or BHKHA-C cells were transfected with C7 or WT RNA. On day 1 and 4 p.t., cells were fixed and stained for E protein expression (using 4G2 antibody). (b) IFA after infection. Supernatant from the RNA-transfected cells on day 4 p.t. was used to infect naive BHK-21 cells. At 24 h p.i., cells were fixed and stained for viral E protein expression. (c) Focus morphology. Viruses (C7t and WT) in the supernatants from transfected BHK-HA-C cells were subjected to focus-forming assay on BHK-21 and BHK-HA-C cells. On day 5 p.i., focus-forming units (FFU) were determined by immunostaining. (d) Virus titers in supernatants of transfected cells on day 4 post-transfection. The limit of detection is 10 FFU/ml. (e) Diagram of passaging C7t virus on BHK-HA-C cells. The C7t virus was continuously passaged on BHK-HA-C cells for 8 rounds, resulting in adaptive P8 C7t virus. (f) Focus morphology of P8 C7t virus on

BHK-HA-C cells. Focus-forming units were assayed on day 5 post-infection. (g) Virus titer of P8 C7t virus. (h) Summary of the whole genome sequence of P8 C7t virus. The sequence of ZIKV strain FSS13025 (KU955593) was used as a reference.

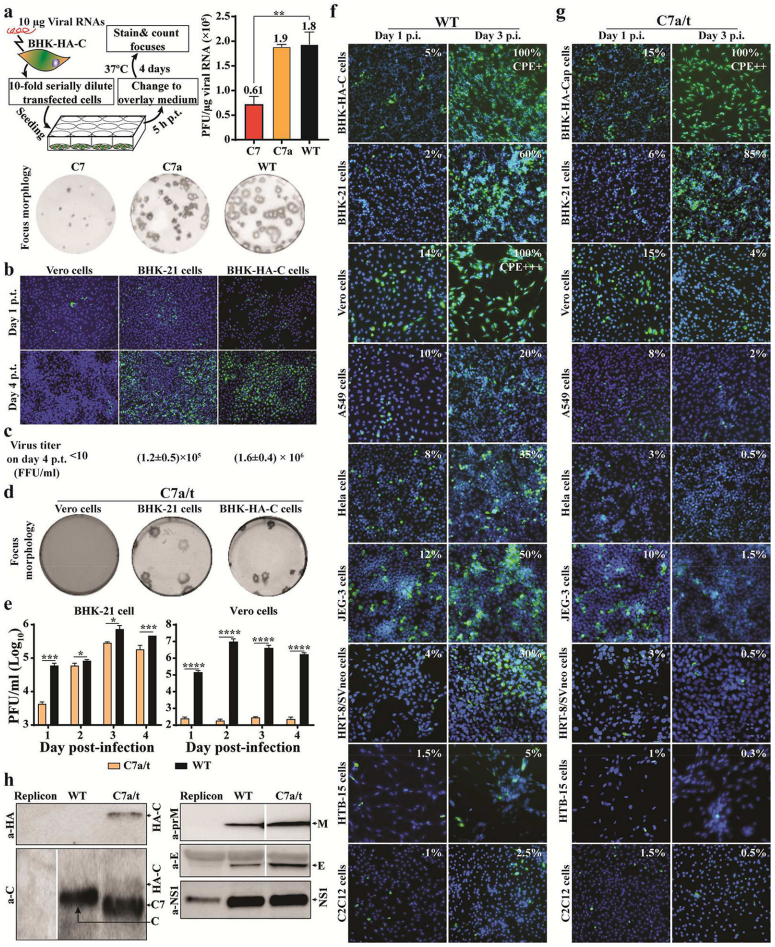

Figure 3.

Characterization of the C7 mutant with adaptive mutations (C7a). (a) Comparison of specific infectivity between C7 and C7a (with adaptive prM E21K and NS2B E27G mutations). Upper-left panel outlines the experimental procedures. Infectious cDNA clone-derived C7 and C7a RNAs were transfected into BHK-HA-C cells. Transfected cells were serially diluted and seeded onto BHK-HA-C cell monolayers. Focus-forming units were detected by immunostaining on day 4 post-transfection. PFU/μg RNA values were calculated and presented in the upperright panel. The lower panel shows the morphology of the foci after immunostaining. Statistically significant differences were determined using a t-test. (b) IFA of RNA-transfected Vero, BHK-21, and BHK-HA-C cells. C7a RNAs (containing the C7 deletion plus prM E21K and NS2B E27G mutations) were electroporated into BHK-21 or BHK-HA-C cells. The viral E protein expression was monitored by IFA. (c) Virus titers in supernatants on day 4 p.t. determined by focus-forming assay. (d) Focus morphology. C7a/t viruses were harvested from the C7a RNA-transfected BHK-HA-C cells on day 4 post-transfection. Focus morphology of C7a/t virus was determined on Vero, BHK-21, and BHK-HA-C cells. (e) Viral replication kinetics. BHK-21 or Vero cells were infected with C7a/t or WT ZIKV at an MOI of 0.5. Virus titers were measured by focus-forming assay on BHK-HA-C cells. Statistical significance was determined using multiple t-test. (f) IFA for monitoring the spread of WT ZIKV infection. (g) IFA for monitoring the spread of C7a/t

virus infection. Cells were infected with WT or C7a/t virus (MOI 0.25). Viral E protein expressing cells were quantified by IFA using 4G2 antibody. Percentages of E-positive cells are presented. CPE, viral infection-mediated cytopathic effect; +, mild; ++, moderate; +++, severe. (h) Western blot analysis of C7a/t virus. Supernatants from replicon RNA-transfected BHK-HA-C cells (day 4 p.t.), WT RNA-transfected Vero cells (day 4 p.t.), and C7a RNA-transfected BHK-HA-C cells (day 4 p.t.) were analyzed for viral proteins (HA-C, C, M, E, and NS1) using Western blotting.

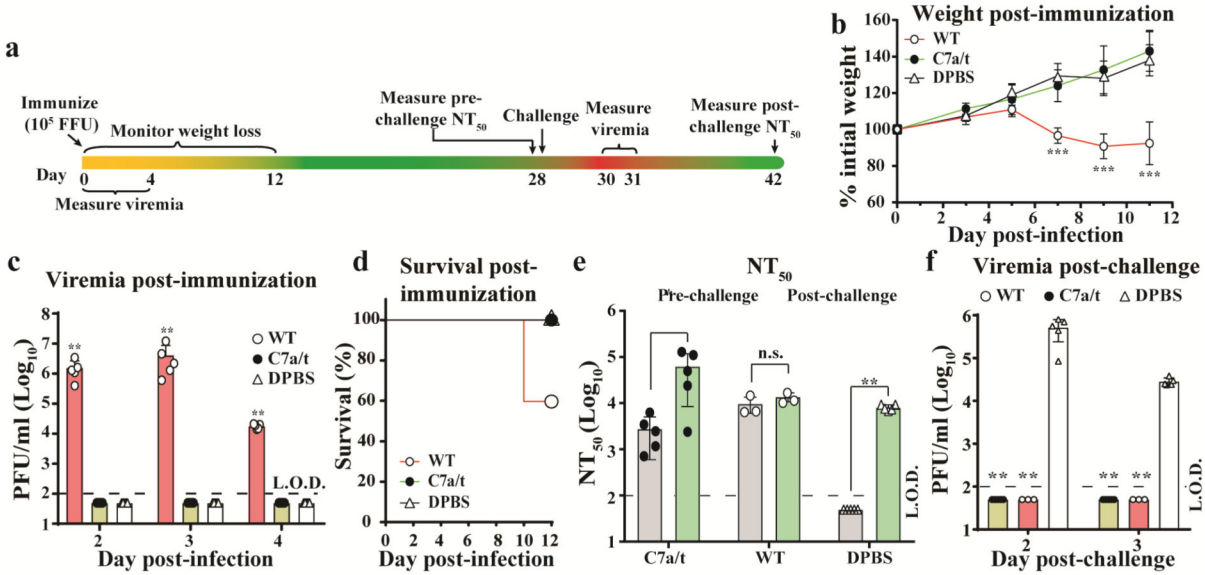

Figure 4.

Single-dose immunization of C7a/t protects A129 mouse from ZIKV infection. (a) Experimental design. Three groups (n=5) of three-week-old A129 mice were subcutaneously injected with C7a/t virus, WT ZIKV, or DPBS (sham). Viremia was monitored from days 2 to 4 post-infection. Following immunization, mice were monitored for weight loss over 12 days. On days 28 and 42 post-immunization, mice were bled and quantified for pre- and post-challenge neutralizing antibody titers (NT_{50}). Mice were subcutaneously challenged with 10^6 PFU of ZIKV PRVABC59 strain on day 28 post-immunization. On days 2 and 3 post-challenge (equivalent to days 30 and 31 post-immunization), mice were bled to measure viremia post-challenge. (b) Mouse weight post-immunization. Two-way ANOVA was used to determine the statistical significance in weight change among groups. (c) Viremia post-immunization. Viremia was determined by focus-forming assay on BHK-HA-C cells. Limit of detection (L.O.D.), 100 PFU/ml. (d) Survival after immunization. (e) Pre-and post-challenge neutralizing antibodies. NT_{50}s were determined by ZIKV/mCherry neutralization assay (see details in Methods). L.O.D., 100 reciprocal sera dilution. (f) Viremia post-challenge. Viremia on days 2 and 3 post-challenge were measured by plaque assay. An unpaired nonparametric Mann-Whitney test was used for analyzing the statistical significance of viremia and NT_{50}s.

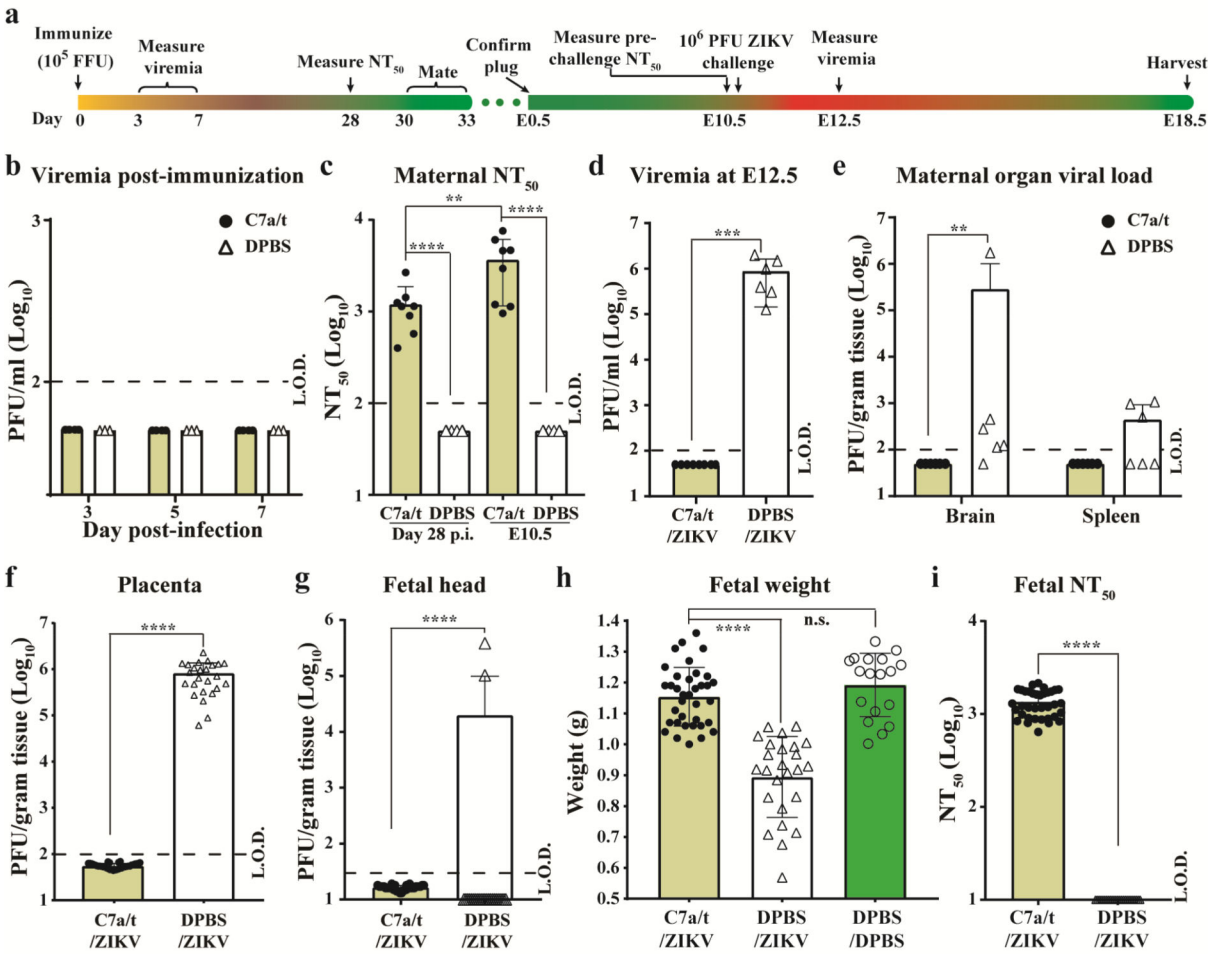

Figure 5.

Prevention from *in utero* transmission of ZIKV in pregnant mice. (a) Experimental design. Three-week-old female A129 mice were subcutaneously inoculated with 10^5 FFU of C7a/t (n=8) or DPBS (sham; n=6). (b) Viremia post-immunization. The viremia was measured on BHK-HA-C cells. (c) Neutralizing antibodies in serum on day 28 post-immunization and E10.5 during pregnancy. (d) Maternal viremia at E12.5 after ZIKV challenge. The pregnant mice were challenged at E10.5 with 10^6 PFU of ZIKV PRVABC59. (e) Viral loads in maternal organs at E18.5. (f) Viral loads in placenta at E18.5. (g) Viral loads in fetal heads at E18.5. (h) Fetal weight at E18.5. (i) Neutralizing antibodies in fetal serum. Viremia was determined by plaque assay. The NT_{50}s were determined by an mCherry ZIKV neutralization assay. An unpaired nonparametric Mann-Whitney test was used for analyzing statistical significance. The L.O.D.s for viremia, tissue virus load, maternal NT_{50}s, and fetal NT_{50}s are 100 FFU/ml, 100 PFU/g tissue, 100 dilution, and 10 dilution, respectively.

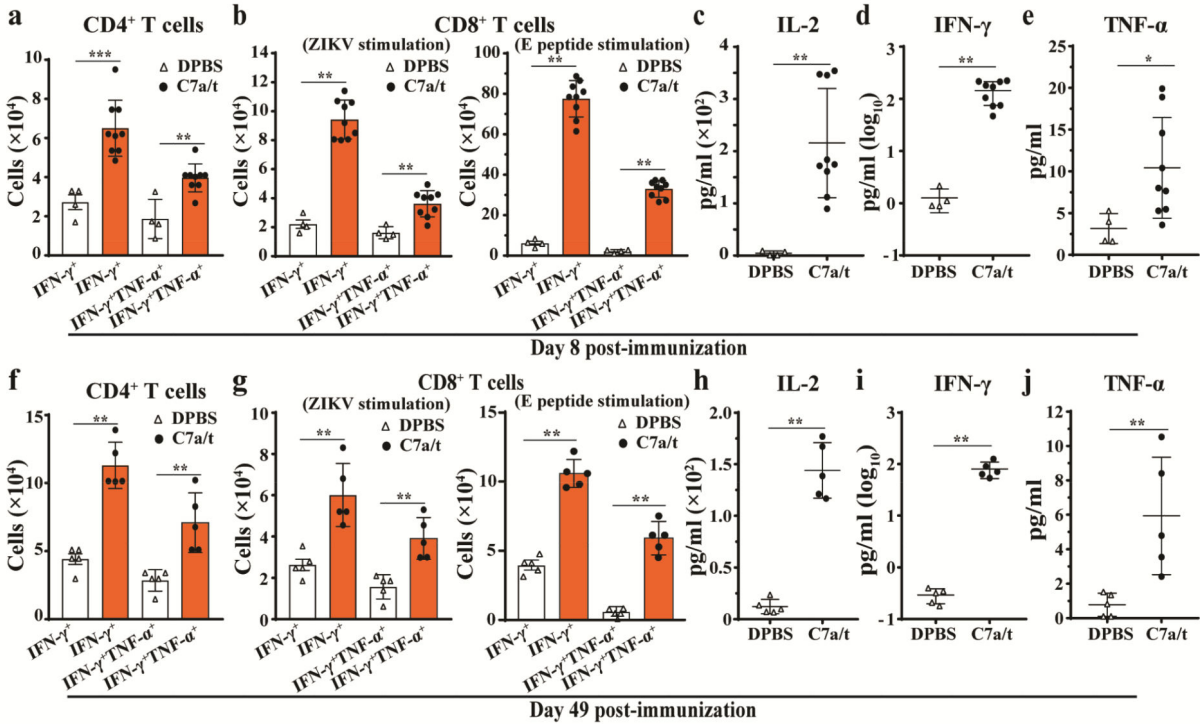

Figure 6.

Robust T cell response in A129 mice after C7a/t immunization. Three-week old A129 mice were subcutaneously inoculated with C7a/t viruses (10^5 FFU) or DPBS (sham). Splenocytes were harvested on days 8 (a-e) and 49 (f-j) post-immunization, cultured *ex vivo* with ZIKV for 24 h or ZIKV E peptide for 5 h, and stained for IFN-γ, TNF-α, and T cell markers. Cytokines (IL-2, IFN-γ, and TNF-α) in splenocyte culture medium were measured by a Bioplex assay following *ex vivo* stimulation with ZIKV for 2 days. (a, f) Total numbers of $CD4^+$ T cell subsets per spleen. Splenocytes were stimulated by ZIKV. (b, g) Total numbers of $CD8^+$ T cell subsets. Splenocytes were stimulated by ZIKV (left panel) or E peptide (right panel). IL-2 (c, h), IFN-γ (d, i), and TNF-α (e, j) in cell culture were measured after splenocytes were stimulated by ZIKV. An unpaired nonparametric Mann-Whitney test was used for analyzing statistical significance.